Volume 9 Number 1 2022

STUDENT JOURNAL OF PHYSICS

INTERNATIONAL JOURNAL

INDIAN ASSOCIATION OF PHYSICS TEACHERS

ISSN – 2319-3166

STUDENT JOURNAL OF PHYSICS

This is a quarterly journal published by Indian Association Of Physics Teachers. It publishes research articles contributed by Undergraduate and Postgraduate students of colleges, universities and similar teaching institutions, as principal authors.

Registered Office
Editor-in-Chief, SJP,
Institute of Physics,
Sainik School, Bhubaneswar,
Odisha, India – 751005
Website: www.iopb.res.in/~sjp/

STUDENT JOURNAL OF PHYSICS

Scope of the Journal

The journal is devoted to research carried out by students at undergraduate level. It provides a platform for the young students to explore their creativity, originality, and independence in terms of research articles which may be written in collaboration with senior scientist(s), but with a very significant contribution from the student. The articles will be judged for suitability of publication in the following two broad categories:

1. **Project based articles**
   These articles are based on research projects assigned and guided by senior scientist(s) and carried out predominantly or entirely by the student.
2. **Articles based on original ideas of student**
   These articles are originated by the student and developed by him/ her with possible help from senior advisor. Very often an undergraduate student producing original idea is unable to find a venue for its expression where it can get due attention. SJP, with its primary goal of encouraging original research at the undergraduate level provides a platform for bringing out such research works.
   It is an online journal with no cost to the author.

Since SJP is concerned with undergraduate physics education, it will occasionally also publish articles on science education written by senior physicists.

Information for Authors

- Check the accuracy of your references.
- Include the complete source information for any references cited in the abstract. (Do not cite reference numbers in the abstract.)
- Number references in text consecutively, starting with [1].

- Language: Papers should have a clear presentation written in good English. Use a spell checker.

Submission

1. Use the link "Submit" of Website to submit all files (manuscript and figures) together in the submission (either as a single .tar file or as multiple files)
2. Choose one of the Editors in the link "Submit" of Website as communicating editor while submitting your manuscript.

Preparation for Submission

Use the template available at "Submit" section of Website for preparation of the manuscript.

Re-Submission

- For re-submission, please respond to the major points of the criticism raised by the referees.
- If your paper is accepted, please check the proofs carefully.

Scope

- SJP covers all areas of applied, fundamental, and interdisciplinary physics research.

Editorial

We are happy to announce that regular publication of Student Journal of Physics has been resumed with the current issue which has been somewhat hampered during the last three years because of the outbreak of pandemic Covid-19 since 2019. During the last three years, academic activities in schools, colleges and universities were seriously affected due to their partial and sometimes complete closure. Since isolation was being mandated and student research is somewhat a collective activity it suffered a serious setback. Now we hope a new dawn has finally arrived and Student Journal of Physics is favourably poised to resume its journey with new vigour and spirit.

During the last year Student Journal of Physics has added two new members to its editorial board:

1. Professor Suresh K Patra, Institute of Physics, Bhubaneswar, India.

2. Professor Joshua Veazey, Grand Valley State University, Michigan, USA.

Also, former editor Professor Prasanta K Panigrahi (IISER, Kolkata, India) will now take on the responsibility of Chief Editor.

L. Satpathy

Skyrme-Hartree-Fock-Bogoliubov calculation of nuclear structure properties in Pt isotopes

Dani Rose J Marattukalam[1] and A.K. Rhine Kumar[2]
Department of Physics, Cochin University of Science and Technology, Kochi - 682022, India.*

Abstract. In this work, we attempt to study the nuclear structure properties of the Pt isotopic chain in the framework of Hartree-Fock-Bogoliubov (HFB) theory. HFB theory is a Self-Consistent Mean Field (SCMF) model[1] that combines the nuclear mean-field Hartree-Fock (HF) theory and the Bardeen-Cooper-Schrieffer (BCS) theory that explains nuclear pairing correlations. We investigate the ground-state properties of the even-even isotopic chain $^{166-260}$Pt. These include the binding energy per nucleon, two-neutron separation energy, quadrupole deformation, proton, neutron and charge radii and neutron skin thickness. We also studied the dependence of neutron skin thickness on the temperature of the system. The code HFBTHO v2.00d[2] that solves the Skyrme HFB equations in the deformed harmonic oscillator basis was used to perform the calculations.

Communicated by Prof. S.D. Mahanti

1. INTRODUCTION

Hartree-Fock-Bogoliubov (HFB) theory is essentially a self-consistent framework generalizing the Hartree-Fock (HF) theory that describes the nuclear mean-field and the Bardeen-Cooper-Schrieffer (BCS) theory that explains nuclear pairing correlations [3]. HFB theory is considered a more general framework for the description of the nuclei than BCS theory as the single-particle wave functions and energies are specified beforehand in the BCS theory in terms of phenomenological mean-field potential, whereas HFB theory incorporates the complete HF theory with the relaxation of particle number conservation [4]. Also a single self-consistent theory was necessary while considering nuclei far from stability as the pairing correlations near the drip lines couldn't be accounted for merely as a residual interaction. In Hartree-Fock-Bogoliubov theory the state of the system is specified by two operators - the one-particle density matrix ρ which is the same as in Hartree-Fock theory and the pairing density matrix κ that describes the Cooper pairing effect [5]. In this work, we have studied the ground state properties of the even-even $^{166-260}$Pt isotopic chain by employing the HFB solver HFBTHO v2.00d [2].

*danimarattukalam95@gmail.com

2. THEORETICAL FRAMEWORK

In this section, we briefly describe the Skyrme-Hartree-Fock-Bogoliubov formalism. In second quantization, the general two-body Hamiltonian is written in terms of the particle creation and annihilation operators ($a^\dagger$, a) as:

$$H = \sum_{mn} e_{mn} a_m^\dagger a_n + \frac{1}{4} \sum_{mnpq} \bar{v}_{mnpq} a_m^\dagger a_n^\dagger a_p a_q \tag{1}$$

where $\bar{v}_{mnpq} = \langle mn|V|pq - qp\rangle$ are the anti-symmetrized two-body interaction matrix elements [6]. The Bogoliubov transformation [7] of the particles to quasi-particles [8] has the form:

$$\begin{pmatrix} \eta^\dagger \\ \eta \end{pmatrix} = \begin{pmatrix} U^T & V^T \\ V^* & U^* \end{pmatrix} \begin{pmatrix} a^\dagger \\ a \end{pmatrix} \tag{2}$$

U and V are the coefficients that transform the single-particle states (n) into quasi-particle states (μ). In the HFB calculations the nuclear ground-state wavefunction is defined as the quasi-particle vacuum i.e., action of quasi-particle annihilation operator on the wavefunction satisfies $\eta_\mu|\phi\rangle = 0$. We define the one-body density matrix ρ and pairing density matrix κ as follows:

$$\begin{aligned} \rho_{mn} &= \langle\phi|a_n^\dagger a_m|\phi\rangle = \sum_\mu V_{n\mu} V_{m\mu}^* \\ \kappa_{mn} &= \langle\phi|a_m a_n|\phi\rangle = \sum_\mu U_{m\mu} V_{n\mu}^* \end{aligned} \tag{3}$$

Performing the variation of energy in eq. (1) with respect to ρ and κ gives the HFB equations:

$$\begin{pmatrix} e + \Gamma - \lambda & \Delta \\ -\Delta^* & -(e + \Gamma)^* + \lambda \end{pmatrix} \begin{pmatrix} U \\ V \end{pmatrix} = E \begin{pmatrix} U \\ V \end{pmatrix} \tag{4}$$

where

$$\Gamma_{ij} = \sum_{kl} \bar{v}_{ikjl} \rho_{lk} \quad \text{and} \quad \Delta_{ij} = \frac{1}{2} \sum_{kl} \bar{v}_{ijkl} \kappa_{lk} \ . \tag{5}$$

The finite temperature HFB equations has a similar form except for the density matrices that now depend on the Fermi-Dirac occupation factor f_μ of the quasi-particle states μ [2].

$$\begin{aligned} \rho &= U f U^T + V(1 - f) V^T \\ \kappa &= U f V^T + V(1 - f) U^T \end{aligned} \tag{6}$$

The HFB energy can be written as:

$$E[\rho, \tilde{\rho}] = \int \mathcal{H}(\nabla) \lceil^\ni \nabla \tag{7}$$

where $\mathcal{H}(\nabla)$ is the local energy density as a function of nuclear densities and their derivatives with time-reversal symmetry. In the Skyrme-HFB approach, the total binding energy is given as a sum of the kinetic energy, the interaction energy between nucleons given by the Skyrme energy density functional, the pairing energy, the Coulomb energy and the correction arising from the spurious motion.

$$E = E_{kin} + \int \varepsilon_{Sk}\, d^3r + E_{pair} + E_{coul} - E_{corr} \tag{8}$$

For even-even nuclei, the Skyrme energy density functional takes the form [2]

$$\varepsilon_{Sk}[\rho] = C_t^{\rho\rho}[\rho]\rho_t^2 + C_t^{\rho\tau}[\rho]\rho_t\tau_t + C_t^{J^2}[\rho]\mathbf{J}_t^2 + C_t^{\rho\Delta\rho}[\rho]\rho_t\Delta\rho_t + C_t^{\rho\nabla J}[\rho]\rho_t\nabla\cdot\mathbf{J}_t \tag{9}$$

with τ_t and $\mathbf{J}_t$ being the kinetic energy density and the spin-current respectively. The coupling constants $C_t^{uu'}$ are functions of local isoscalar density $\rho_0(r)$ which are fitted to the data. We consider pairing correlations to arise from contact delta forces and hence the pairing energy density is given as

$$E_{pair} = \frac{1}{2}V_0\left[1 - V_1\left(\frac{\rho}{\rho_0}\right)^{\gamma}\right]\sum_q \tilde{\rho}_q^2 \tag{10}$$

where $\tilde{\rho}$ is the pairing local density with the index q labeling the neutron ($q = n$) or the proton ($q = p$). V_0 and V_1 are the coupling constants for pairing interaction.

The protons also experience a Coulomb potential due to their electric charges and hence the energy density will also have contributions from the Coulomb energy. The Coulomb energy has an exchange term apart from the usual direct term. The exchange term arises from the anti-symmetric nature of fermionic wavefunctions and is calculated using Slater approximation.

$$E_{Coul}^{dir} = \frac{e^2}{2}\iint d^3r d^3r' \frac{\rho_{ch}(\mathbf{r})\rho_{\mathbf{ch}}(\mathbf{r}')}{|\mathbf{r}-\mathbf{r}'|} \tag{11}$$

$$E_{Coul}^{ex} = -\frac{3}{4}e^2\left(\frac{3}{\pi}\right)^{1/3}\int d^3r\rho_{ch}^{4/3}(\mathbf{r}) \tag{12}$$

This form of the Energy Density Functional (EDF) can be used in the HFB equation obtained in eq. (4) to give the Skyrme-Hartree-Fock-Bogoliubov equations.

3. RESULTS

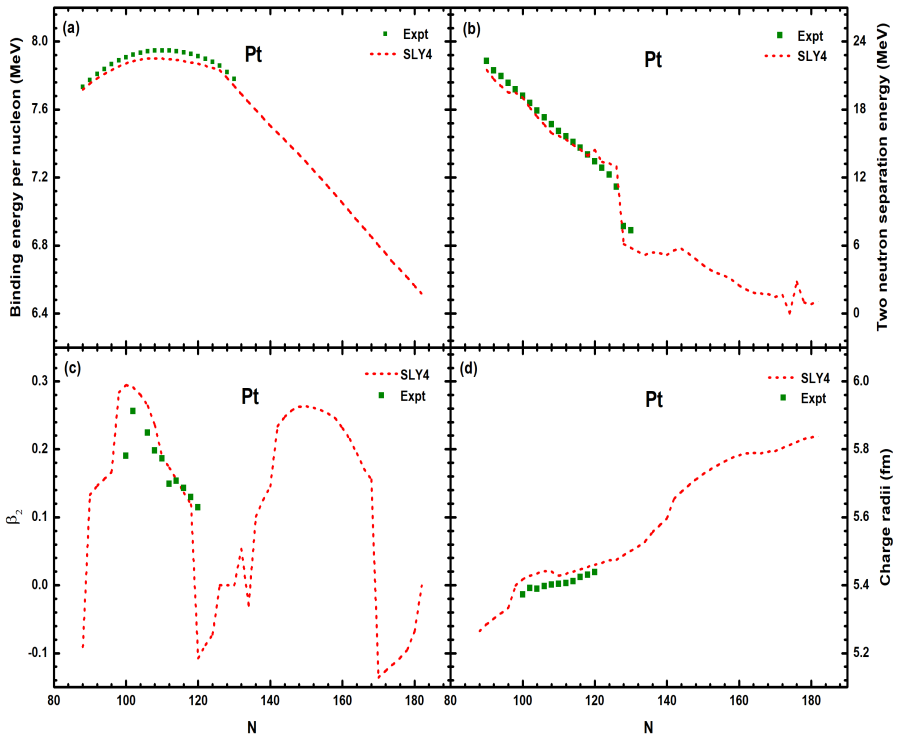

Figure 1. The (a) binding energy per nucleon, (b) two neutron separation energy, (c) the quadrupole deformation parameter, β_2 and (d) the charge radii calculated for the even-even isotopic chain $^{166-260}$Pt are plotted as a function of neutron number, N along with the experimental values [10–12].

Figure 1 shows the ground state properties of Pt isotopic chain, the binding energy per nucleon, the two-neutron separation energy, the quadrupole deformation parameter and the charge radii obtained using the Skyrme parameter set SLY4 [9]. We have used SLY4 parameterization as it was developed to give accurate results for neutron matter and nuclei far from stability. The calculated values are found to agree well with the experimental observations [10–12].

The binding energy per nucleon for the isotopic chains $^{166-260}$Pt are found to be within a range of 0.05 MeV of the experimental values. The difference is lower near the drip lines suggesting that SLY4 parameterization works well near the drip lines which was expected.

The two-neutron separation energy of a nucleus is defined as the energy required to separate two

neutrons from the nucleus. A sharp decrease is found in the value of two-neutron separation energy at the magic number 126. Thus, it requires large energies to disrupt magic nuclei.

The quadrupole deformation β_2 of the nucleus is a general measure of its shape about the axially symmetric axis and determines the value of other parameters like quadrupole moment. The calculated values validate the fact that magic nuclei are generally spherical with $\beta_2 = 0$. This can be seen here for the magic neutron number 126.

The charge radius of a nucleus is defined as:

$$R_{ch} = \sqrt{R_p^2 + 0.64}\,. \tag{13}$$

This depends on the proton radius (R_p) and is usually a measure of the size of the nucleus. The charge radius indicates the proton distribution within the nucleus.

The proton radii and neutron radii are defined as the root mean square values of the respective density distributions.

$$< R_{\rm q}^2 >= \frac{\int r^2 \rho_{\rm q}(\vec{r}, T) d\vec{r}}{\int \rho_{\rm q}(\vec{r}, T) d\vec{r}} \tag{14}$$

Here, the densities are normalized to give the respective particle numbers,

$$\int \rho_q(\vec{r}, T) d\vec{r} = Q, \quad Q = Z, N; \text{ and } T \text{ represents the temperature.} \tag{15}$$

Thus, the proton and neutron radii are:

$$R_{\rm n} =< R_{\rm n}^2 >^{1/2} \qquad R_{\rm p} =< R_{\rm p}^2 >^{1/2} \tag{16}$$

The proton and neutron radii are calculated for the even-even isotopic chain $^{166-260}$Pt. Owing to the increasing number of neutrons as the mass number increases we also find an increase in the neutron radius.

The neutron skin thickness is an important parameter in nuclear physics, especially for exotic nuclei. This is defined as the difference between the neutron radii and the proton radii. We observe that the neutron skin depth increases with the neutron number and hence obtain an outer crust for heavier isotopes that is devoid of the protons, often called the neutron skin. So neutron-rich nuclei are often considered as an interesting tool, which connects finite and infinite nuclear matter. Here, we investigate the dependence of neutron skin thickness on the temperature. Fig. 2 shows the neutron skin thickness as a function of neutron number, N for different temperatures. The neutron skin thickness increases markedly with the increase in temperature. Hence, temperature plays a crucial role in neutron skin formation. This can be attributed to the occupation probabilities of the single-particle states around the Fermi level that varies with temperature [13]. As temperature increases higher unoccupied energy levels tend to be occupied causing larger proton and neutron radii. This leads to an increase in the neutron skin thickness.

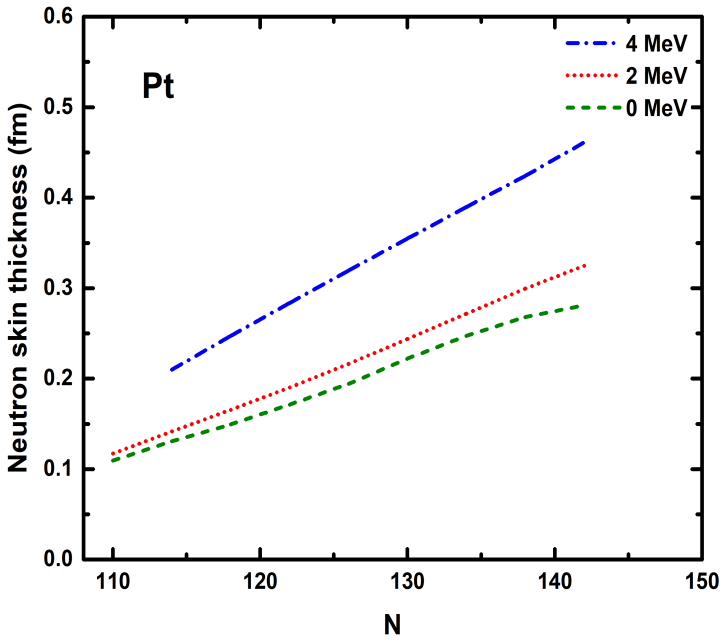

Figure 2. Neutron skin thickness as a function of neutron number, N at temperatures T = 0 MeV, T = 2 MeV and T = 4 MeV calculated for the even-even isotopic chain $^{188-222}$Pt.

4. CONCLUSION

We have calculated the ground-state as well as the excited state properties of the $^{166-260}$Pt isotopic chain using Skyrme-Hartree-Fock-Bogoliubov theory. Our results are in good agreement with the available experimental data. Further, we would like to extend our work to more systems, both finite nuclei and infinite nuclear matter, and the work is under progress.

ACKNOWLEDGEMENTS

A.K.R.K. acknowledges the financial support provided by the Department of Science and Technology (DST), India, via the DST-INSPIRE Faculty award.

References

[1] M. Bender, P.-H. Heenen, and P.-G. Reinhard, Rev. of Mod. Phys. **75**, 121 (2003).

[2] M. Stoitsov et al., Comp. Phys. Comm. **184**, 1592 (2013).

[3] J. Dobaczewski, H. Flocard and J. Treiner, Nucl. Phys. A **422**, 103 (1984).

[4] D.J. Rowe, *Nuclear Collective Motion: Models and Theory*, Methuen and Co. Ltd., London (1970).

[5] Mathieu Lewin and Sverine Paul, ESAIM: Math. Model. Numer. Anal. **48**, 5386 (2013).

[6] M. Stoitsov, J. Dobaczewski, W. Nazarewicz, and P. Ring, Comp. Phys. Comm. **167**, 43 (2005).

[7] N. N. Bogolyubov, Soviet Phys. Usp. **2**, 236 (1959).

[8] Walid Younes, Daniel Marc Gogny, and Jean-François Berger, *A microscopic theory of fission dynamics based on the generator coordinate method*, **950**, Springer International Publishing, Switzerland (2019).

[9] E. Chabanat, P. Bonche, P. Haensel, J. Meyer, and R. Schaeffer, Nucl. Phys. A, **635**, 231 (1998).

[10] M. Wang et al., Chin. Phys. C **45**, 030003 (2021).

[11] T. Belgya et al., *Handbook for calculations of nuclear reaction data*, RIPL-2. **IAEA-TECDOC-1506**, IAEA, Vienna (2006).

[12] I. Angeli and K. P. Marinova, At. Data Nucl. Data Tables **99**, 69 (2013).

[13] A. N. Antonov et. al., Phys. Rev. C **95**, 024314 (2017).

A Study on Nuclear Pairing using BCS Theory

Nabeel Salim and A.K. Rhine Kumar
Department of Physics, Cochin University of Science and Technology, Kochi - 682022, India. *

Abstract. Pairing correlation in nuclei is recognized as the dominant many-body correlation beyond the nuclear mean-field. It was suggested by the occurrence of nuclear phenomena like the odd-even mass staggering (OES) and an energy gap of 1-2 MeV between the ground state and the lowest single-particle excitation. In this work, we have studied the temperature dependence of the pairing gap in ^{94}Sr & ^{120}Sn[1,2]. The single-particle energies are calculated using the Nilsson Model and the pairing strength ($G_{p,n}$) by equating the pairing gap to the empirical pairing gap. The average pairing gap is found to vanish after the critical temperature. In the case of ^{120}Sn the proton pairing is found to be exactly zero at all temperatures (magic nuclei). The empirical pairing gap is extracted from OES[3]. The five-point formula is used for a global calculation of both proton and neutron pairing gap over the entire nuclear landscape, with the binding energy data taken from the Atomic Mass Evaluation 2020[4]. The empirical pairing gap data is grouped into four categories; even-even, odd-neutron, odd-proton and odd-odd. Each group is fitted with a power function aZ^b and aN^b for proton and neutron pairing respectively and the parameters are found. The overall fit in mass number (A) shows the power (b) to be $-\frac{1}{3}$ rather than the $-\frac{1}{2}$ from the accepted $12/\sqrt{A}$ law.

Communicated by Prof. S.D. Mahanti

1. INTRODUCTION

Pairing plays a crucial role in superconducting solids where it was first introduced by Bardeen, Cooper and Schrieffer [5]. This same theory was developed in the case of nuclei by Bohr, Mottelson and Pines [6] and Belyaev [7]. Bardeen, Cooper and Schrieffer (BCS) theory gives an approximate wave function for the pairing Hamiltonian and can be used to explain well-bound nuclei. In BCS theory two nucleons with the same quantum numbers except for the projection of their spin on the same axis interact attractively leading to a lower energy state. In section 2 we derive the FTBCS gap equation from the grand potential [1,2]. This gap equation along with particle number equation can be solved numerically and study the change in pairing gap with temperature. The empirical pairing gap can be calculated from odd-even mass staggering (OES) [3,8]. In section 3.1, the proton and neutron pairing gap of ^{94}Sr & ^{120}Sn are calculated using the finite temperature BCS equation

*nabeel.salim12@gmail.com

(FTBCS) . In section 3.2, we present the neutron and proton pairing gaps at zero temperature, these data are fitted with a power function aZ^b and aN^b for proton and neutron pairing respectively. The fitted parameters are given in Tables 1 & 2.

2. THEORETICAL FRAMEWORK

BCS theory was the first microscopic theory of superconductivity developed in 1957 [5]. It explained superconductivity in metals as the effect of condensation of Cooper pairs, which is the pairing of electrons near the Fermi level through the interaction with the crystal lattice. This coupling interaction is mediated by phonons. In BCS theory pairing takes place between electrons with opposite momenta and opposite spin ($+k$ up,$-k$ down). The pairs overlap strongly and form a condensate.

Similar phase transition behaviour is observed in atomic nuclei. In the case of nuclei, compared to a superconducting metal, it is finite and small. Secondly, there is not yet a reliable microscopic nuclear many-body theory where one can derive the pairing interaction and its strength. So to write the Hamiltonian of a nuclear system, we consider a single-particle model of non-degenerate orbitals $\nu\,(n, l, j, m_j)$. The pairing Hamiltonian of a system of nucleons interacting with the pairing force and having zero total angular momentum is written as follows [1,2].

$$\hat{H} = \sum_{\nu>0}(e_\nu - \lambda - E_\nu) + 2\sum_{\nu>0} E_\nu f_\nu + \frac{\Delta^2}{G} \tag{1}$$

Where *G* is the constant pairing strength, Δ is the pairing gap, λ is the Lagrange multiplier and also the chemical potential, e_ν is the single-particle energy, E_ν is the quasi-particle energy and f_ν is the Fermi-Dirac distribution function for quasi-particles.

$$E_\nu = \sqrt{(e_\nu - \lambda)^2 + \Delta^2} \tag{2}$$

$$f_\nu = \frac{1}{1 + e^{\beta E_\nu}} \tag{3}$$

The grand potential is defined as

$$\Omega = ln\left(Tr\left\{\exp(-\beta\hat{H})\right\}\right) \tag{4}$$

By substituting Eq. (1) in Eq. (4) we get.

$$\Omega = -\beta\sum_{\nu>0}(e_\nu - \lambda - E_\nu) + 2\sum_{\nu>0} ln\left[1 + \exp(-\beta E_\nu)\right] - \beta\frac{\Delta^2}{G} \tag{5}$$

The standard choice for the gap parameter (Δ) is the value that minimizes the grand potential (Ω), so by minimizing Ω we get the finite temperature BCS gap equation.

$$\frac{\partial\Omega}{\partial\Delta} = \beta\sum_{\nu>0}\frac{\Delta}{E_\nu} - 2\sum_{\nu>0}\frac{\exp(-\beta E_\nu)}{1 + \exp(-\beta E_\nu)}\frac{\beta\Delta}{E_\nu} - 2\beta\frac{\Delta}{G} = 0 \tag{6}$$

$$\sum_{\nu>0} \frac{1}{E_\nu} \left(1 - 2\frac{\exp(-\beta E_\nu)}{1+\exp(-\beta E_\nu)}\right) = \frac{2}{G} \tag{7}$$

The expression inside the bracket of Eq. (7) can be simplified as $\tanh\left(\frac{\beta E_\nu}{2}\right)$

$$\frac{2}{G} = \sum_{\nu>0} \frac{1}{E_\nu} \tanh\left(\frac{\beta E_\nu}{2}\right) \tag{8}$$

Similarly, the particle number expression can be derived from grand potential Ω.

$$N = \frac{\partial \Omega}{\partial \alpha} \tag{9}$$

Where $\alpha = \beta\lambda$

$$N = \sum_{\nu>0} \left[1 - \frac{(e_\nu - \lambda)}{E_\nu} \tanh\left(\frac{\beta E_\nu}{2}\right)\right] \tag{10}$$

Eq. (8) & Eq. (10) can be solved numerically. The dependence of Δ on T can be found. For a particular temperature, Δ becomes zero and is called critical temperature T_c. So Δ varies from $\Delta_0 \to 0$ as T varies from $0 \to T_c$.

3. RESULTS

3.1 FTBCS pairing gap

The pairing gap is calculated for ^{94}Sr & ^{120}Sn. We have found the single-particle energies of the nuclei from the Nilsson model. The maximum effect of pairing happens at $T = 0$ MeV, this is found by OES. The energy levels which are affected by the pairing are taken in summation which is close to the Fermi level. The levels are fixed and the pairing strength is adjusted so that the pairing gap matches the empirical odd-even staggering at $T = 0$ MeV.

3.1.1 Strontium - ^{94}Sr

The proton pairing strength (G_p) of ^{94}Sr can be found by adjusting the proton pairing gap at zero temperature ($\Delta_p(0)$) to OES, which gives $G_p = 0.2803$ MeV and $\Delta_p(0) = 1.4961$ MeV. Similarly, we get $G_n = 0.18604$ MeV and $\Delta_n(0) = 1.0059$ MeV. The energy levels taken are $N_1 = 4, N_2 = 35$ and $N_1 = 14, N_2 = 45$ respectively. Where $N_1 \& N_2$ are lower and upper limits of the energy levels taken in the FTBCS equations.

3.1.2 Tin - ^{120}Sn

In the case of ^{120}Sn, $Z = 50$ is a magic number (closed shell), there is no proton pairing due to the shell closure. Where as the neutron pairing is present as $N = 70$, the G_n value of ^{120}Sn can be

found by adjusting $\Delta_n(0)$ to OES, which gives $G_n = 0.2019$ MeV and $\Delta_n(0) = 1.3918$ MeV. The energy levels taken are $N_1 = 10, N_2 = 41$ and $N_1 = 18, N_2 = 52$ respectively.

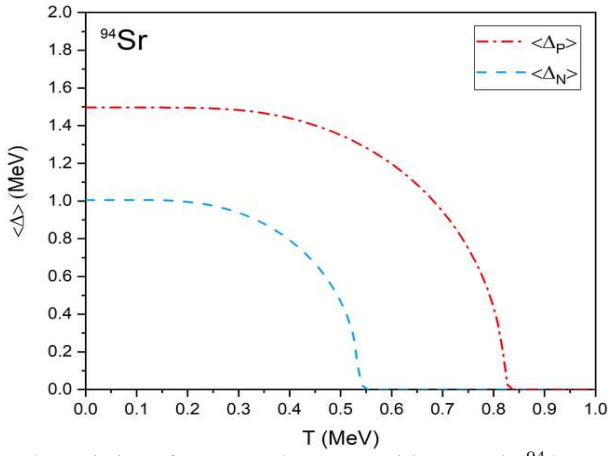

Figure 1. The variation of proton and neutron pairing gaps in ^{94}Sr nucleus with the temperature is presented. The critical temperature, $T_c = 0.8282$ MeV for proton pairing and $T_c = 0.5455$ MeV for neutron pairing.

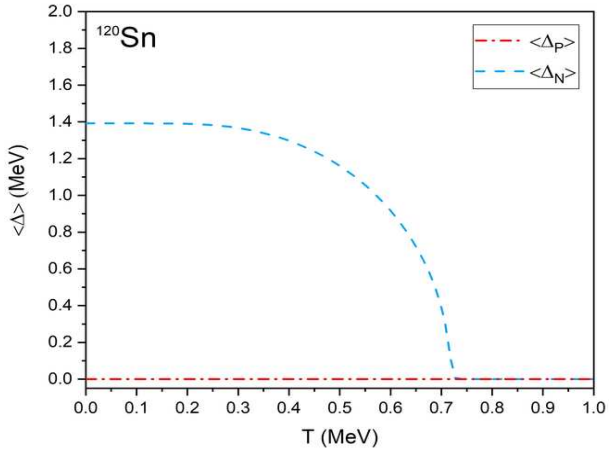

Figure 2. Same as Fig. 1, but for the nucleus ^{120}Sn. The critical temperature, $T_c = 0.7273$ MeV for neutron pairing and no proton pairing.

3.2 Empirical pairing gap

The empirical pairing gap is found using the five-point formula given in [3,8]. The binding energy data is taken from Atomic Mass Evaluation 2020 [4]. Neutron and proton pairing gaps are evaluated separately and fitted with function aX^b where X=N, Z respectively. Then the average pairing gap

is found and fitted with function aA^b. Where a & b are fitting parameters. We exclude nuclei with a mass number (A) less than 16. In Figures 3 & 4 pairing gaps are fitted to neutron and proton numbers respectively. The numerical values of the fitting parameters are included in Tables 1 & 2.

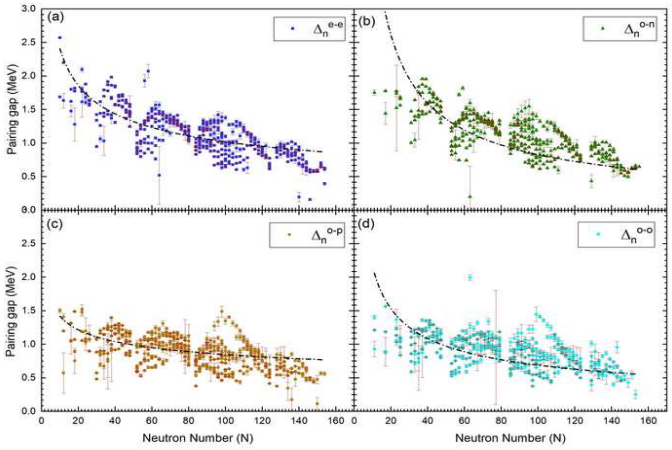

Figure 3. The neutron pairing gap of the following nuclei are calculated and fitted. (a) Even-even nuclei (Δ_n^{e-e}). (b) Odd-neutron nuclei (Δ_n^{o-n}). (c) Odd-proton nuclei (Δ_n^{o-p}). (d) Odd-odd nuclei (Δ_n^{o-o}). The black dash-dotted line is determined by fitting to the data using the function aN^b.

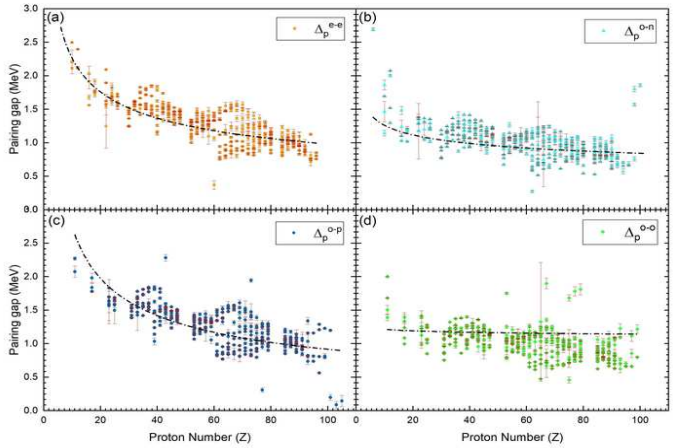

Figure 4. The proton pairing gap of the following nuclei are calculated and fitted. (a) Even-even nuclei (Δ_p^{e-e}). (b) Odd-neutron nuclei (Δ_p^{o-n}). (c) Odd-proton nuclei (Δ_p^{o-p}). (d) Odd-odd nuclei (Δ_p^{o-o}). The black dash-dotted line is determined by fitting to the data using the function aZ^b.

Table 1. The fittings of empirical neutron pairing gaps in even-even, odd-N, odd-Z and odd-odd nuclei from five point formula as functions of N and the corresponding root-mean-square deviation and coefficient of determination R^2 (with 95% confidence bounds).

Group of Nuclei	Number of Nuclei	parameter of the pairing gap function aN^b		RMS Deviation (σ)	R square
		a $\pm\Delta$ a	b $\pm\Delta$ b		
Even-even	424	5.682 ± 0.221	-0.373 ± 0.011	0.341	0.741
Odd-Neutron	384	22.124 ± 1.584	-0.713 ± 0.018	0.317	0.830
Odd-Proton	445	2.377 ± 0.024	-0.224 ± 0.002	0.236	0.935
Odd-odd	410	6.764 ± 0.473	-0.496 ± 0.011	0.234	0.640

Table 2. The fittings of empirical proton pairing gaps in even-even, odd-N, odd-Z and odd-odd nuclei from five point formula as functions of Z and the corresponding root-mean-square deviation and coefficient of determination R^2 (with 95% confidence bounds).

Group of Nuclei	Number of Nuclei	parameter of the pairing gap function aZ^b		RMS Deviation (σ)	R square
		a $\pm\Delta$ a	b $\pm\Delta$ b		
Even-even	378	5.211 ± 0.195	-0.362 ± 0.011	0.340	0.737
Odd-Neutron	378	1.886 ± 0.108	-0.175 ± 0.017	0.265	0.233
Odd-Proton	339	8.223 ± 0.482	-0.476 ± 0.016	0.309	0.743
Odd-odd	346	1.293 ± 0.063	-0.027 ± 0.014	0.219	0.010

4. CONCLUSION

The dependence of temperature on the pairing is studied using the finite-temperature BCS theory. We have plotted the average pairing gap with temperature for ^{94}Sr & ^{120}Sn. The G value (Pairing strength) for protons is found to be greater than neutrons as expected. The proton pairing is larger than neutron pairing as it is equated to OES. The proton pairing of ^{120}Sn is found to be zero which is exact for low pairing strength as Tin is a magic nucleus in proton number. The critical temperature on average is also related to Δ_0 as $T_c = 0.53\Delta_0$ for neutron and proton pairing. Above these critical temperature we found that the pairing to be zero.

We have calculated empirical nuclear pairing using the five-point formula and fitted it with a power function. The five-point formula reduces most of the effects from the persisting mean-field than the previously used three-point formula. A global calculation for both proton and neutron pairing gap over the entire nuclear landscape has been performed with the binding energy data from Atomic Mass Evaluation 2020 [4]. From these fits, we found that except for the proton pairing of odd-neutron nuclei (Fig. 4 (b)) and odd-odd nuclei (Fig. 4 (d)), the power function is giving a very good fit. The poor fit for these cases may indicate the presence of a constant term in the fitted function. We haven't checked the dependence of neutron excess $(\mathrm{N}-\mathrm{Z})$ in pairing. An overall fit corresponding to all nuclei groups to a function of mass number (A) is fitted. The result is $(4.609 \pm 0.014)A^{-0.33}$ which is a $-\frac{1}{3}$ dependence rather than the $-\frac{1}{2}$ from the accepted $12/\sqrt{A}$ law. This implies a weaker dependence on pairing gap than the usual [9], and The current result supports a $-\frac{1}{3}$ law [10].

ACKNOWLEDGMENTS

A.K.R.K. acknowledges the financial support provided by the Department of Science and Technology (DST), India, via the DST-INSPIRE Faculty award.

References

[1] L. Moretto, Nucl. Phys. A **185**, 145 (1972).

[2] L. Moretto, Phys. Lett. B **35**, 379 (1971).

[3] D. G. Madland and J. Nix, Nucl. Phys. A **476**, 1 (1988).

[4] M. Wang, W. Huang, F. Kondev, G. Audi, and S. Naimi, Chin. Phys. C **45**, 030003 (2021).

[5] J. Bardeen, L. N. Cooper, and J. R. Schrieffer, Phys. Rev. **108**, 1175 (1957).

[6] A. Bohr, B. R. Mottelson, and D. Pines, Phys. Rev. **110**, 936 (1958).

[7] S. T. Belyaev, Kgl. Danske Videnskab. Selskab. Mat.-Fys. Medd. (1959).

[8] P. Moller and J. Nix, Nucl. Phys. A **536**, 20 (1992).

[9] W. Satua, J. Dobaczewski, and W. Nazarewicz, Phys. Rev. Lett. **81**, 3599 (1998).

[10] S. Hilaire, J. F. Berger, M. Girod, W. Satua, and P. Schuck, Phys. Lett. B **531**, 61 (2002).

Relevance of infinite nuclear matter quantities in finite nuclei

Praveen K. Yadav[1]*, Raj Kumar[1] and M. Bhuyan[2,3]

[1]School of Physics and Materials Science, Thapar Institute of Engineering and Technology, Patiala-147004, Punjab, India

[2]Center for Theoretical and Computational Physics, Department of Physics, Faculty of Science, University of Malaya, Kuala Lumpur 50603, Malaysia

[3]Institute of Research and Development, Duy Tan University, Da Nang 550000, Vietnam

Abstract. The density-dependent symmetry energy depicts the energy difference between the binding energy of symmetric nuclear matter and pure neutron matter, which is associated with various phenomena such as exotic nuclei, heavy ion-collision experiments, supernovae, and gravitational collapse in neutron stars. In this theoretical work, we study the isospin-dependent properties of finite nuclei, namely symmetry energy, surface symmetry energy, volume symmetry energy, and their ratio κ from their corresponding components available in the infinite nuclear matter using the coherent density fluctuation model. We have performed the calculations for a few $even-even$ isotopes of Titanium for the non-linear NL3 parameter set within the purview of relativistic mean-field formalism. This study provides theoretical understanding and computational steps for analyzing the magicity of Titanium nuclei which can be extended to different sets of nuclei across the nuclear landscape.

Communicated by Prof. S.K. Patra

1. INTRODUCTION

While moving across from nuclear landscape from stable to unstable exotic nuclei, the appearance of newer magic numbers and the disappearance of others can be observed owing to the distinct constituents of the nucleon-nucleon interaction. Some of these nuclei have widely different nuclear configurations than those predicted from early nuclear models. These nuclei can have extreme values of neutron-proton asymmetry (also referred as isospin-asymmetry) which is given as $\delta = (\rho_n - \rho_p)/\rho$, where ρ_n and ρ_p are the neutron and proton densities respectively and $\rho = \rho_n + \rho_p$ is the baryon density. The $\rho-$ meson term handles the density type isospin, whereas the $\delta-$ meson handles the mass asymmetry.

*praveenkumarneer@gmail.com

The fundamental problem of understanding nuclear physics involving isospin is describing the equation of states (EOS) in terms of binding energy per nucleon

$$E(\rho,\delta) = E(\rho,0) + E_{sym}(\rho)\delta^2 + \mathcal{O}(\delta^{\triangle}).....,\tag{1}$$

The term $E(\rho,0)$ refers to energy in a symmetric nuclear matter which depends on the total density, i.e., the sum of neutron and proton densities. $E_{sym}(\rho)$ refers to the density-dependent nuclear symmetry energy (NSE). δ^4 is found to be very small and can be safely ignored [1,2] and thus, the EOS can be described using the parabolic equation. The study of NSE has a profound research interest in the field of nuclear astrophysics. It is used to characterize both the finite and infinite asymmetric nuclear matter. However, proper study related to the density-dependence of symmetry energy is still in a nascent stage. Recently Bhuyan *et al.* [3-7] have successfully studied various density-dependent symmetry energy properties using the relativistic mean-field formalism, providing a newer direction in this field. Moreover, the availability of radioactive ion beam (RIB) and its advances in measurements of exotic nuclei has given experimental support and stimulated theoretical research projects towards understanding the properties related to nuclear symmetry energy.

The structure of the paper is as follows: The theoretical formalism pertaining to the relativistic mean-field formalism is discussed in Section 2.1. We then present the need and derivation for calculating the symmetry energy and its related parameter using the coherent density fluctuation model in Section 2.2. Section 3 provides a flowchart detailing the steps for creating the required program. Finally, we present the calculations and a brief discussion of the result for nuclear symmetry energy, surface, and volume symmetry energy for Titanium nuclei in Section 4.

2. METHODOLOGY

2.1 Relativistic mean-field formalism

The relativistic mean-field (RMF) formalism has various advantages corresponding to its non-relativistic counterparts [8-12]. The RMF formalism includes the presence of spin-orbit interaction in the relativistic equations. This method has successfully reproduced the bulk properties of finite nuclei such as binding energy, quadrupole moment, charge radius, etc., throughout the mass table. It also considers some of the meson-nucleon coupling parameters, which successfully reconciles with the experimental data. Moreover, the nuclear equation of state and properties associated with neutron stars can be studied using this formalism. A generalized expression of non-linear finite-range RMF model having typical Lagrangian density takes the form as

$$\begin{aligned}\mathcal{L} = {} & \overline{\psi}\{i\gamma^{\mu}\partial_{\mu} - M\}\psi + \frac{1}{2}\partial^{\mu}\sigma\partial_{\mu}\sigma - \frac{1}{2}m_{\sigma}^2\sigma^2 - \frac{1}{3}g_2\sigma^3 - \frac{1}{4}g_3\sigma^4 - g_s\overline{\psi}\psi\sigma \\ & -\frac{1}{4}\Omega^{\mu\nu}\Omega_{\mu\nu} + \frac{1}{2}m_w^2\omega^{\mu}\omega_{\mu} - g_w\overline{\psi}\gamma^{\mu}\psi\omega_{\mu} - \frac{1}{4}\vec{B}^{\mu\nu}.\vec{B}_{\mu\nu} + \frac{1}{2}m_{\rho}^2\vec{\rho}^{\mu}.\vec{\rho}_{\mu} \\ & -g_{\rho}\overline{\psi}\gamma^{\mu}\vec{\tau}\psi\cdot\vec{\rho}^{\mu} - \frac{1}{4}F^{\mu\nu}F_{\mu\nu} - e\overline{\psi}\gamma^{\mu}\frac{(1-\tau_3)}{2}\psi A_{\mu}.\end{aligned}\tag{2}$$

Here the fields for the electromagnetic, ρ, σ and ω meson is depicted as A_μ, $\vec{\rho}_\mu$, σ and ω_μ respectively. Moreover, $\vec{B}_{\mu\nu}$, $\Omega^{\mu\nu}$ and $F^{\mu\nu}$ are the field tensors corresponding to the $\vec{\rho}_\mu$, ω^μ and photon fields respectively.

Within RMF formalism, the simplistic expression of nuclear symmetry energy can be written as:

$$S^{NM}(\rho) = \frac{1}{2}\frac{\partial^2(\mathcal{E}/\rho)}{\partial\alpha^2}\bigg|_{\alpha=0}, \tag{3}$$

where $\mathcal{E}$ is the energy density and α corresponds to the neutron-proton asymmetry in terms of baryon density. Following Ref. [3, 13-16] the mesons coupling corresponding to the fields of nucleons can be given as

$$g_i(\rho) = g_i(\rho_{sat})f_i(x)|_{i=\sigma,\omega}. \tag{4}$$

Here

$$f_i(x) = a_i\frac{1+b_i(x+d_i)^2}{1+c_i(x+d_i)^2}, \tag{5}$$

and

$$g_\rho = g_\rho(\rho_{sat})e^{a_\rho(x-1)}, \tag{6}$$

where $x = \rho/\rho_{sat}$. The term ρ_{sat} refers to saturation density of nuclear matter.

This project involves the use of baryon densities from the relativistic mean-field approach for a specific parametrization to calculate the value of symmetry energy. We have chosen the most popular and well-known NL3 parameter set for our endeavour because it has proven to reproduce nuclear saturation properties that are in excellent agreement with the present experimental data throughout the periodic table [4-5, 17-19] and references therein. The main task was then to create a program from scratch which could calculate the isospin dependent properties of finite nuclei such as symmetry energy and the different parameters directly associated with it, namely volume symmetry energy, surface symmetry energy, and their ratios κ at local density.

2.2 Coherent density fluctuation model

The symmetry energy is a property associated with infinite nuclear matter which is defined in momentum space, whereas finite nuclei is defined in coordinate space [20-24]. Experimentally it is not possible to observe the symmetry energy. However, we can evaluate this property using observables related to it. For this task, different models were proposed, including liquid drop model (LDM) [25], coherent density fluctuation model (CDFM) [21,22], etc. The nuclei in the LDM are assumed to be macroscopic drops of nuclear matter in the form of liquid which is incompressible. This model accounts for the short-range nuclear interactions as well as the nuclear matter saturation property.

According to this, for a finite nucleus, the symmetry energy is strongly correlated with the surface contribution, which implies that a single parameter for all nuclei that are fitted may yield only the average values. Therefore, for evaluating symmetry energy, one needs to take into account the contribution owing to the mass number. However, using additional parameters turns out to be a difficult task in known nuclei, which has a constrained range. Therefore, alternative models for symmetry energy calculation are much needed. The CDFM is one such model that is built upon the Fermi gas model, which has the generator coordinate with long-range collective type correlations. This model was developed by Antonov *et al.* [20,21]. It has successfully calculated the density distribution, ground and excited state root-mean-square (*rms*) radius for different nuclei, namely ^{4}He, ^{16}O, ^{40}Ca, etc. There are many advantages attributed to using CDFM. Firstly, CDFM automatically accounts for fluctuations present due to the density distribution by using the weight function. Secondly, the fluctuations attributed to momentum distribution close to the surface are taken care of using the Wigner distribution function (or mixed density matrix). The one-body density matrix (OBDM) $\rho(\mathbf{r}, \mathbf{r})$ can be represented by another OBDM that has coherent superposition $\rho_x(\mathbf{r}, \mathbf{r})$ corresponding to the fluctons (spherical pieces of nuclear matter).

$$\rho_x(\mathbf{r}) = \rho_0(x)\Theta(x - |\mathbf{r}|), \tag{7}$$

Here, $\rho_x(r)$ is the diagonal part of the OBDM and $\rho_0(x)$ is the spherical flucton density which is expressed as $\rho_0(x) = \frac{3A}{4\pi x^3}$. According to the definition of density matrix, one particle density is given by its diagonal elements [26]: $\rho(\mathbf{r}) = \rho(\mathbf{r}, \mathbf{r'})|_{\mathbf{r'}\rightarrow\mathbf{r}}$. Thus, the infinite superposition of spherical fluctons defined for generator coordinate with radius x containing the Fermi gas of all uniformly distributed nucleons with mass A, the OBDM then takes the form as [22,26]:

$$\rho(\mathbf{r}, \mathbf{r'}) = \int_0^\infty dx|\mathcal{F}(\S)|^{\in}\rho_{\S}(\mathbf{r}, \mathbf{r'}). \tag{8}$$

The term $\mathcal{F}(\S)|^{\in}$ is called as the weight function where $\rho_x(\mathbf{r}, \mathbf{r}')$ depicts the coherent OBDM superposition which is described as:

$$\rho_x(\mathbf{r}, \mathbf{r}') = \mathbf{3}\boldsymbol{\rho}_\mathbf{0}(\mathbf{x})\frac{\mathbf{J_1}(\mathbf{k_F}(\mathbf{x})|\mathbf{r} - \mathbf{r}'|)}{(\mathbf{k_F}(\mathbf{x})|\mathbf{r} - \mathbf{r}'|)} \times \Theta\left(x - \tfrac{|\mathbf{r}+\mathbf{r}'|}{2}\right). \tag{9}$$

The Bessel function J_1 has the order as one. The term $k_F(x)$ depicts Fermi momentum for radius x of the flucton given as

$$k_F(x) = \left(\frac{3\pi^2}{2}\rho_0(x)\right)^{1/3} \equiv \frac{\beta}{x}, \tag{10}$$

where

$$\beta = \left(\frac{9\pi A}{8}\right)^{1/3} \simeq 1.52A^{1/3}. \tag{11}$$

The Wigner distribution function corresponding to OBDM is given as

$$W(\mathbf{r},\mathbf{k}) = \int_0^\infty dx|\mathcal{F}(\S)|^{\in}\mathcal{W}_\S(\mathbf{r},\mathbf{k}), \tag{12}$$

where $W_x(\mathbf{r},\mathbf{k}) = \frac{4}{8\pi^3}\Theta(x-|\mathbf{r}|)\Theta(k_F(x)-|\mathbf{k}|)$. Similarly applying the CDFM approach, the density term $\rho(r)$ can be stated as

$$\begin{aligned}\rho(r) &= \int d\mathbf{k}W(\mathbf{r},\mathbf{k}) \\ &= \int_0^\infty dx|\mathcal{F}(\S)|^{\in}\frac{\ni\mathcal{A}}{\triangle\pi\S^{\ni}}\times(\S-|\mathbf{r}|).\end{aligned} \tag{13}$$

$$|\mathcal{F}(\S)|^{\in} = -\left(\frac{\infty}{\rho_\prime(\S)}\frac{\lceil\rho(\nabla)}{\lceil\nabla}\right)_{\nabla=\S}. \tag{14}$$

The normalization of weight function is given as $\int_0^\infty dx|\mathcal{F}(\S)|^{\in} = \infty$. Using Ref. [3, 22, 27, 28], the expression of symmetry energy for asymmetric nuclear matter as a function of $\rho_0(x)$ takes the form

$$S^{NM} = 41.7\rho_0^{2/3}(x) + b_1\rho_0(x) + b_2\rho_0^{4/3}(x) + b_3\rho_0^{5/3}(x). \tag{15}$$

Here b_1, b_2 and b_3 are constants derived from the method of Bruckner *et al.* [29, 30] having the values given as

$$\begin{aligned}b_1 &= 148.26, \\ b_2 &= 372.84, \\ b_3 &= -769.57.\end{aligned} \tag{16}$$

The expression for effective symmetry energy for asymmetric nuclear matter S from CDFM can be stated as [3, 22, 27, 28]:

$$S = \int_0^\infty dx|\mathcal{F}(\S)|^{\in}\mathcal{S}^{\mathcal{NM}}(\S). \tag{17}$$

Brueckner's energy density functional method suggests that in some areas the symmetry energy shows negative values, which is physically not possible. So to avoid such non-physical negative values of symmetry energy, one needs to set proper limits of integration in the Eq. 17. This is one of the most crucial parts of programming. Following Ref. [23], we first introduce the minimum value of nuclear distance x_{min} at which symmetry energy for asymmetric nuclear matter changes sign from negative value (at $x < x_{min}$) to positive value (at $x > x_{min}$). For $x < x_{min}$ the value of weight function is nearly zero, which implies that no contribution to the symmetry energy is supplied in this region. Moreover, it is required to introduce the value of x_{max} beyond which the weight function contribution to symmetry energy is negligible. This is done by first defining $\Delta x = x_{max} - x_{min}$.

Later we put the constraint for the value of x_{max} to be the point at which $S - S_{\Delta x} \leq 0.1$ MeV. Here the term $S_{\Delta x}$ is evaluated using the Eq. 17. Thus, the expression in Eq. 17 can be better written as

$$S = \int_{x_{min}}^{x_{max}} dx|\mathcal{F}(\S)|^{\in}\mathcal{S}^{\mathcal{NM}}(\S). \tag{18}$$

Using the Bethe-Weizsäcker LDM, the symmetry energy can be expressed in terms of surface and volume components which can be stated as [31],

$$S = \frac{S_V}{1 + \frac{S_S}{S_V}A^{-1/3}} = \frac{S_V}{1 + \frac{1}{\kappa A^{1/3}}} \tag{19}$$

The term $\kappa \equiv \frac{S_V}{S_S}$ is defined as the ratio of volume and surface symmetry energy. One can evaluate the volume and surface components of symmetry energy separately as

$$S_V = S\left(1 + \frac{1}{\kappa A^{1/3}}\right) \tag{20}$$

and

$$S_S = \frac{S}{\kappa}\left(1 + \frac{1}{\kappa A^{1/3}}\right), \tag{21}$$

Following Ref. [32,33] it is possible to find the expression of symmetry energy S and κ as a function of nuclear saturation density ρ_0 within the CDFM formalism as

$$S = S(\rho_0)\int_0^{\infty} dx|\mathcal{F}(\S)|^{\in}\left[\left(\frac{\rho(\S)}{\rho_\prime}\right)^{\gamma}\right], \tag{22}$$

and

$$\kappa = \frac{3}{R\rho_0}\int_0^{\infty} dx|\mathcal{F}(\S)|^{\in}\S\rho_\prime(\S)\left[\left(\frac{\rho_\prime}{\rho(\S)}\right)^{\gamma} - \infty\right]. \tag{23}$$

The term $S(\rho_0)$ is the symmetry energy at saturation density, and R is the nuclear matter radius. It is crucial to note here that the term ρ_0 corresponds to nuclear saturation density, whereas $\rho_0(x)$ corresponds to spherical flucton density as a function of nuclear distance (x). Here γ parameter is chosen to be 0.3, as it is consistent with the various experimental results [32-34]. Using the same integration limits of symmetry energy i.e. x_{min} and x_{max}, we next evaluate the value of κ from Eq. 23. This permits us to finally evaluate the value of volume symmetry energy and surface symmetry energy by following Eqs. 20, 21 respectively. Thus, the computational steps can be summarized as follows: first, one needs to evaluate the symmetry energy within the proper limits using Eq. 18. Subsequently, one needs to find the κ using the Eq. 23. Finally, volume and surface symmetry energy can be evaluated using Eq. 20 and 21 respectively.

3. Flowchart

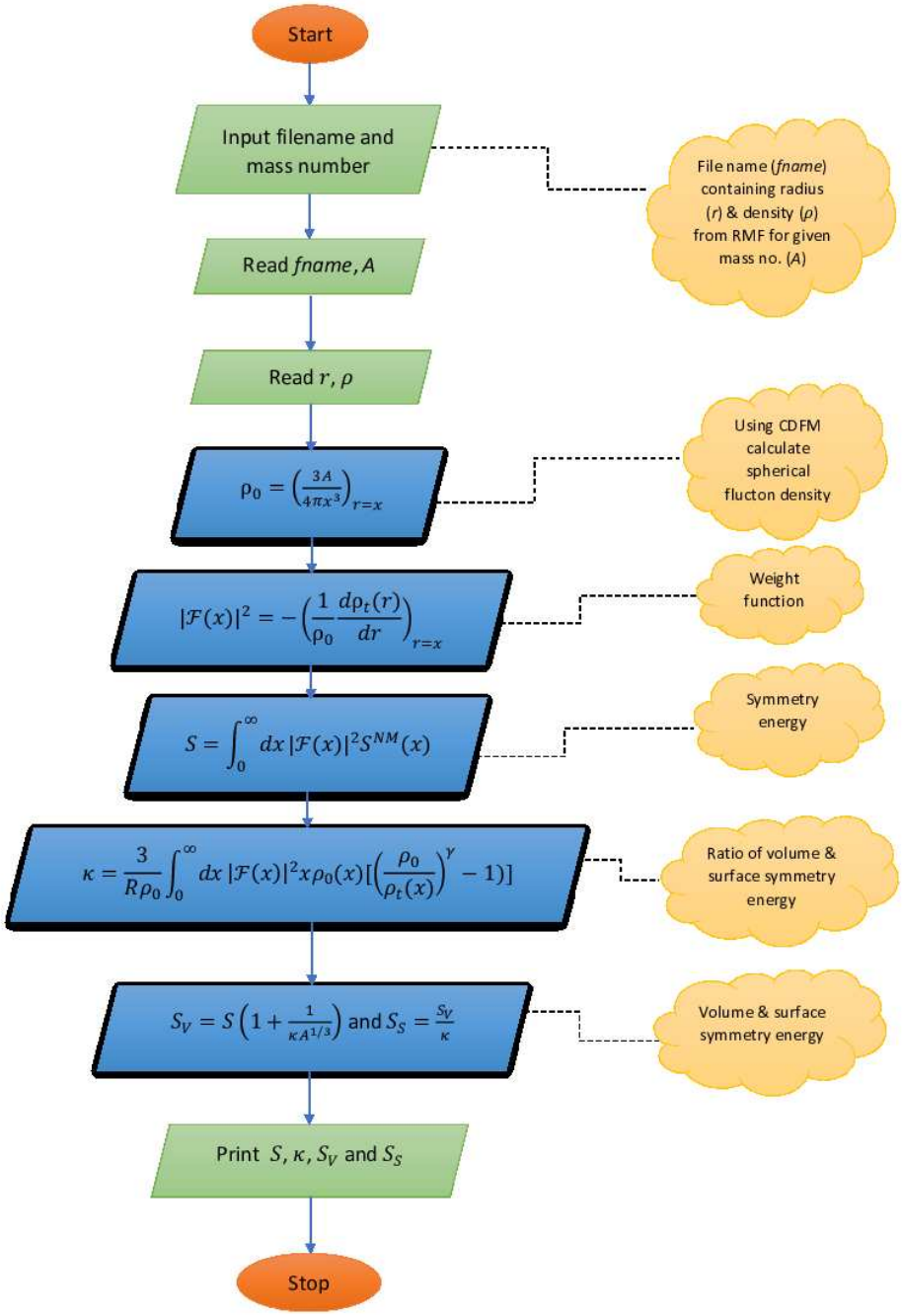
Start
Input filename and mass number
File name (fname) containing radius (r) & density (ρ) from RMF for given mass no. (A)
Read fname, A
Read r, ρ
$\rho_0 = \left(\frac{3A}{4\pi x^3}\right)_{r=x}$
Using CDFM calculate spherical flucton density
$|\mathcal{F}(x)|^2 = -\left(\frac{1}{\rho_0}\frac{d\rho_t(r)}{dr}\right)_{r=x}$
Weight function
$S = \int_0^\infty dx\,|\mathcal{F}(x)|^2 S^{NM}(x)$
Symmetry energy
$\kappa = \frac{3}{R\rho_0}\int_0^\infty dx\,|\mathcal{F}(x)|^2 x\rho_0(x)[\left(\frac{\rho_0}{\rho_t(x)}\right)^\gamma - 1)]$
Ratio of volume & surface symmetry energy
$S_V = S\left(1 + \frac{1}{\kappa A^{1/3}}\right)$ and $S_S = \frac{S_V}{\kappa}$
Volume & surface symmetry energy
Print S, κ, S_V and S_S
Stop

4. RESULTS AND CONCLUSION

In this section, we provide the results and brief discussions related to symmetry energy and its related components, namely volume and surface symmetry energy along with their ratio κ for neutron-rich $even-even$ Titanium isotopes using the relativistic mean-field model for the NL3 parameter set. The coherent density fluctuation model is used to translate the nuclear matter quantities at local density. In other words, the CDFM is used to obtain a transparent relationship for the quantities corresponding to the intrinsic analytical equation of states while using a simple approach to the weight function [24]. The expression of weight function $\mathcal{F}(\S)^{\in}$ given in Eq. 14, may seem to be of simple nature. However, this expression provides a pathway to correlate the infinite matter quantities such as symmetry energy and its related surface and volume components existing in momentum space to that of the corresponding finite nuclear quantities in the coordinate space. Within the relativistic mean-field model, the symmetry energy, which is a quantity of infinite nuclear matter, can directly be calculated for any finite nucleus from the difference of isoscalar and isovector parts of the energy density functional. This questions the need to implement the CDFM model instead of the relativistic mean-field equation to calculate the symmetry energy for finite nuclei. It can be owed to the fact that many parameters such as pairing, shell corrections and other meson interactions are unaccounted for when performing the calculations for the finite nuclei, which leads to poor description of the symmetry energy in finite nuclei. To counter this problem, CDFM provides a uniform description of finite nuclei similar to infinite nuclear matter through the primary assumption of nuclear matter as spherical pieces of nuclear matter known as fluctons [35]. For calculating the value of symmetry energy at local density, we need to obtain the values of total density (sum of neutron and proton density) as a function of nuclear distance. We have plotted the total baryon density distribution, i.e., the sum of proton density ρ_p and neutron density ρ_n as a function of nuclear distances, for few Titanium nuclei based on NL3 parameter in Fig 1. A similar characteristic of nuclear density is observed for all the presented nuclei.

After finding the values of total baryon density as a function of nuclear distance, we use the CDFM to find the value of weight function $\mathcal{F}(\S)^{\in}$ from Eq. 14 for each of the isotopic nuclei. It can be observed that the magnitude of the weight function is always less than one. The plot of total densities as a function of nuclear distance for some of the nuclei is given in Fig. 1. A thorough investigation of Fig. 1 suggests that an increase in proton number (Z) yields slight enhancement in the surface region. Hence, effective nuclear matter quantities can be understood by using the total density distribution. The plot of weight function $\mathcal{F}(\S)^{\in}$ as a function of nuclear distance is provided in Fig. 2. Some inference based on Fig. 2 can be drawn, which states that the shape of weight function corresponds to a bell shape having maximum density near the middle of flucton radius which is not necessarily the center of flucton. Since the weight function is dependent on total density, the increase or decrease in the value of total density leads to the corresponding increase or decrease in the weight function.

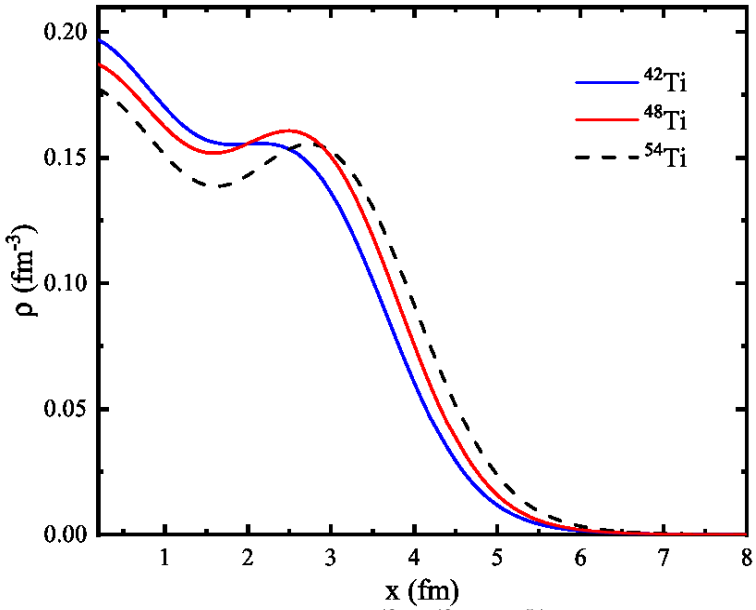

Figure 1. Total density distribution for ^{42}Ti, ^{48}Ti and ^{54}Ti isotopes from NL3 as a function of nuclear distances. Follow the text for details.

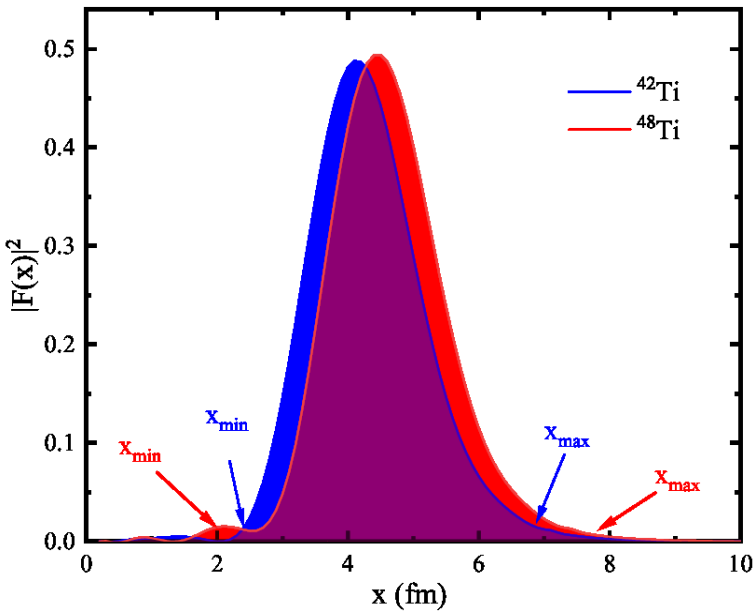

Figure 2. Weight function corresponding to ^{42}Ti and ^{48}Ti isotopes from NL3 as a function of nuclear distance. Follow the text for details.

The principal aim of this project involved the calculations pertaining to the symmetry energy and

its volume and surface components. Symmetry energy being a quantity of infinite nuclear matter, cannot be measured directly. However, it is possible to measure it using other observables which share some indirect relationship with it. The isospin asymmetry is the difference in the densities of neutrons and protons. The symmetry energy, which is defined as the energy density derivative with respect to isospin asymmetry, plays a significant role in a range of nuclear physics branches involving the study of ground-state nuclear structure [36-38], heavy-ion reaction dynamics [39,40] and study related to neutron stars [2, 41-43].

Using the value of symmetry energy, we compute the value of its components, namely surface and volume symmetry energy, which are usually calculated at saturation based on the properties of nuclear matter. Based on the method of Brueckner's energy density functional [29,30], some non-physical (negative values) of nuclear symmetry energy were observed. Therefore, this method requires assigning a proper limit to the integration for the calculation of symmetry energy and its related parameter based on the change in sign from negative to positive value detailed in Section 2.2.

We have provided a detailed flowchart as a means of simplifying the whole process of programming for calculating the symmetry energy and its related parameters in Section 3. Moreover, Fig. 2 shows the calculated weight function as a function of nuclear distance for two Titanium isotopes namely ^{42}Ti and ^{48}Ti nuclei. The points x_{min} and x_{max} signify the integration limits for each of the nuclei taken while calculating the value of symmetry energy. Using Titanium isotopic chain and following Eq. 17, 20, 21, and 23, we have calculated the symmetry energy, volume symmetry energy, surface symmetry energy and their ratio κ, respectively, for the NL3 parameter set within the RMF formalism. The values corresponding to these parameters are given in Table 1. The present calculation can be extended to more isotopic chains, including light, heavy and super-heavy regions. The symmetry energy co-efficient, namely, neutron pressure and curvature, can also be incorporated based upon the model of CDFM. These nuclear matter quantities can be treated as primary observable for shell/sub-shell closure (s) at and/or near the drip-line region of the nuclear chart.

Table 1. The calculated symmetry energy (S), volume symmetry energy (S_V), surface symmetry energy (S_S) and their ratio κ for Titanium isotopic chain from non-linear NL3 parameter set is shown in the table

Nucleus	Symmetry energy	Volume symmetry energy	Surface symmetry energy	κ
^{42}Ti	26.54807791	31.80804655	21.90635807	1.452000668
^{44}Ti	26.89762324	32.16993464	22.26152446	1.44509127
^{46}Ti	27.2649504	32.56214504	22.66766852	1.43650173
^{48}Ti	27.60654222	32.88987599	22.87557569	1.437772602
^{50}Ti	27.87674081	33.17500314	23.22874705	1.428187369
^{52}Ti	27.81287292	32.99695584	22.95625787	1.437383916
^{54}Ti	27.75016038	32.85276579	22.83300272	1.438828094

From the Table 1 at ^{50}Ti, which corresponds to N = 28, one can observe a significant increase in the symmetry energy along with its surface and volume components while showing a decrement in κ value, which altogether indicates higher stability of isotopes and a possible shell closure. This will open the path for a better understanding of the properties across the nuclear landscape. A few investigations in the direction of isospin dependent effective nuclear surface quantities for possible signature of magicity or shell/subshell closure are already established in Ref. [3] and references therein.

Acknowledgements

One of the authors, PKY would like to acknowledge Thapar Institute of Engineering and Technology, Patiala, India, and University of Malaya, Kuala Lumpur, Malaysia, for their incentives and support throughout this project.

References

[1] Z.-y. Ma and L. Liu, Phys. Rev. C 66, 024321 (2002).

[2] A.W. Steiner, M. Prakash, J.M. Lattimer, and P.J. Ellis, Phys. Rep. 411, 325 (2005).

[3] M. Bhuyan, B. V. Carlson, S.K. Patra, and S.-G. Zhou, Phys. Rev. C 97, 024322 (2018).

[4] M. Kaur, A. Quddus, A. Kumar, M. Bhuyan, and S.K. Patra, J. Phys. G: Nucl. Part. Phys. 47, 105102 (2020).

[5] M. Kaur, A. Quddus, A. Kumar, M. Bhuyan, and S.K. Patra, Nucl. Phys. A 1000, 121871 (2020).

[6] N. Biswal et al., Astron. Nachr. 342, 462 (2021).

[7] S. K. Biswal et al., Nucl. Phys. A 1004, 122042 (2020).

[8] B.D. Serot and J.D. Walecka (Springer US, Boston, MA, 1992) pp. 4992.

[9] R. Brockmann and R. Machleidt, Phys. Rev. C 42, 1965 (1990).

[10] B.D. Serot and J.D. Walecka, Int. J. Mod. Phys. E 06, 515 (1997).

[11] R. Fritz, H. Mther, and R. Machleidt, Phys. Rev. Lett. 71, 46 (1993).

[12] A.R. Bodmer, Nucl. Phys. A 526, 703 (1991).

[13] J. Boguta and A.R. Bodmer, Nucl. Phys. A 292, 413 (1977).

[14] B.V. Carlson and D. Hirata, Phys. Rev. C 62, 054310 (2000).

[15] G. A. Lalazissis, S. Karatzikos, R. Fossion, D. P. Arteaga, A. V. Afanasjev, and P. Ring, Phys. Lett. B 671, 36 (2009).

[16] T. Nikic, D. Vretenar, P. Finelli, and P. Ring, Phys. Rev. C 66, 024306 (2002).

[17] M. Bhuyan, Phys. Rev. C 92, 034323 (2015).

[18] A. Quddus, M. Bhuyan, S. Ahmad, B. V. Carlson, and S. K. Patra, Phys. Rev. C 99, 044314 (2019).

[19] A. Quddus, M. Bhuyan, and S. K. Patra, J. Phys. G: Nucl. Part. Phys. 47, 045105 (2020).

[20] A. N. Antonov, V. A. Nikolaev, and I. Z. Petkov, Bulg. J. Phys.; (Bulgaria) 6:2 (1979).

[21] A. N. Antonov, V. A. Nikolaev, and I. Z. Petkov, Zeitschrift fr Physik A Atoms and Nuclei 304, 239 (1982).

[22] M. K. Gaidarov, A. N. Antonov, P. Sarriguren, and E. Moya de Guerra, Phys. Rev. C 84, 034316 (2011).

[23] M. K. Gaidarov, A. N. Antonov, P. Sarriguren, and E. M. de Guerra, Phys. Rev. C 85, 064319 (2012).

[24] M. K. Gaidarov, A. N. Antonov, P. Sarriguren, and E. M. de Guerra, AIP Conf. Proc. 1606, 180 (2014).

[25] P. Ring and P. Schuck, The nuclear many-body problem (Springer-Verlag, New York, 1980).

[26] A. N. Antonov, V. A. Nikolaev, and I. Z. Petkov, Z. Phys. A 297, 257 (1980).

[27] A. N. Antonov, D. N. Kadrev, and P. E. Hodgson, Phys. Rev. C 50, 164 (1994).

[28] P. Sarriguren, M. K. Gaidarov, E. M. d. Guerra, and A. N. Antonov, Phys. Rev. C 76, 044322 (2007).

[29] K. A. Brueckner, J. R. Buchler, S. Jorna, and R. J. Lombard, Phys. Rev. 171, 1188 (1968).

[30] K. A. Brueckner, J. R. Buchler, R. C. Clark, and R. J. Lombard, Phys. Rev. 181, 1543 (1969).

[31] P. Danielewicz and J. Lee, Nucl. Phys. A 818, 36 (2009).

[32] P. Danielewicz, Nucl. Phys. A 727, 233 (2003).

[33] P. Danielewicz, arXiv:nucl-th/0411115 (2006).

[34] A. E. L. Dieperink and P. Van Isacker, Eur. Phys. J. A 32, 11 (2007).

[35] S. Ban, J. Meng, W. Satula, and R. A. Wyss, Phys. Lett. B 633, 231 (2006).

[36] T. Nikic, D. Vretenar, and P. Ring, Phys. Rev. C 78, 034318 (2008).

[37] N. V. Giai, B. V. Carlson, Z. Ma, and H. Wolter, J. Phys. G: Nucl. Part. Phys. 37, 064043 (2010).

[38] E. Van Dalen and H. Mther, Int. J. Mod. Phys. E 19, 2077 (2010).

[39] L.-W. Chen, C. M. Ko, B.-A. Li, and G.-C. Yong, Int. J. Mod. Phys. E 17, 1825 (2008).

[40] B.-A. Li, L.-W. Chen, and C. M. Ko, Phys. Rep. 464, 113 (2008).

[41] F. J. Fattoyev, W. G. Newton, J. Xu, and B.-A. Li, Phys. Rev. C 86, 025804 (2012).

[42] M. Dutra, O. Loureno, J. S. S Martins, A. Delfino, J. R. Stone, and P. D. Stevenson, Phys. Rev. C 85, 035201 (2012).

[43] M. Dutra et al., Phys. Rev. C 90, 055203 (2014).

Electrical Characterization of Aluminum (Al) Thin Films

Pragathi M.S.[1], **Vijayakumar G.**[2], **Sunanda S.**[3]

[1]M.Sc. II, Department of Physics, Maharani Cluster University, Bangalore-560001, Karnataka

[2]Associate professor, Department of Physics, Maharani Cluster University, Bangalore-560001, Karnataka *

[3]Assistant professor, Department of Physics, Maharani Cluster University, Bangalore-560001, Karnataka

Abstract. his paper deals with the preparation of aluminum (Al) thin films on glass substrate by thermal evaporation method. The electrical conductivity of the prepared thin films as a function of film thickness was systematically investigated. The electrical conductivity was obtained by the measurement of current and voltage through four-point probe. This study shows that electrical conductivity increases linearly with film thickness in the range of thickness studied in this work.

Communicated by Prof. S.D. Mahanti

1. INTRODUCTION

Aluminum (Al) is the most abundant metal in the earths crust and is the third most abundant element after oxygen (O_2) and silicon (Si). It is silvery white in color, shows high electrical and thermal conductivity and has a melting point of 660^0C. Al has been widely used for various applications. Al films evaporated on substrates are the most commonly used surface coatings for aspheric mirrors since Al is a good light reflector in the visible region and an excellent reflector in the mid and far infrared (IR) regions [1]. Besides, Al is widely used in the microelectronics technology as Ohmic contacts, Schottky barrier contacts, gate electrodes and also as interconnects [2].

Al also finds its application in the fabrication of thin film transistors (TFTs), photo detectors, solar cells and many other devices [3]. In the fabrication of solar cells, Al is heavily used as back contacts due to its ease of deposition, Low sheet resistance and its capability to introduce back surface field effects (BSF) that could minimize carrier recombination rates at the rear side of device [4,5]. In thin film solar cell, high reflectance property of the Al contacts is exploited to serve as a light-trapping solution where low energy photons will be obliquely reflected back into the absorber layer. This increases the optical path length of the light (photons) in the device there by increasing absorption

*vijaykumarbhs1283@gmail.com

efficiency, photocurrent generation, and quantum efficiency of the thin film solar cells particularly in the long wavelength region [6].

Deposition of Al contacts can be carried out by several physical vapor deposition (PVD) methods such as thermal evaporation, electron beam (e-beam) evaporation and also sputtering [7]. Since Al has a fairly low melting point (660^0C), thermal evaporation appears to be good enough for its deposition. In addition, thermal evaporation is the simplest and the most cost-effective compared to the other techniques which makes it a more appealing option.

Even though extensive research has been carried out on the evaporation of Al as contacts in bulk and thin films solar cells. Most of the research activities employ either wafers or glass materials as substrates [8]. Al back contacts which are also used on polymeric materials like polyimide (PI) and polyethylene terephthalate (PET) plastic substrates, still in their infancy phase. Both PI and PET are excellent polymeric materials. They have attracted interests of many parties in photo voltaic (PV) and other related fields due to their reasonable temperature resistance, flexibility, light-weight, low-cost properties [9].

2. THEORY

The sheet resistance Rs is given by

$$Rs = \left(\frac{V}{I}\right) k \tag{1}$$

Where Rs is the sheet resistance (in Ω), V is the dc voltage across the voltage probes, I is the constant dc current passing through the current probes, and k is the correction Factor [10,11]. For more conductive metal films and semi conducting films, it is common to place all electrodes on the same film surface. Such measurements employ terminals-2 to pass current and 2 to pass voltage. A very convenient way to measure the sheet resistance of a film is to press a 4-point- metal tip probe assembly into the surface as shown in Fig.1. The outer probes are connected to current source and inner probes to detect the voltage drop.

Electrostatic analysis of the electric potential and field distributions within the film yields,

$$R = \frac{(\rho X L)}{(wXt)} = R_s \left(\frac{L}{W}\right)$$

where sheet resistance $R_s = \rho/t$.
Resistivity

$$\rho = (R_s \times t) = \left(\frac{k \times V \times t}{I}\right)$$

i.e. resistivity $\rho = R_s x t(\mu\Omega - cm)$ where t stands for thickness, R_s sheet resistance is independent of film dimension other than thickness, k is a constant dependent on the configuration and spacing of the probes. If the thickness of the film is very small as compared to the probe spacing, then

$$k = \frac{\pi}{ln2} = 4.53$$

Thus, sheet resistance,

$$R_s = 4.53\left(\frac{V}{I}\right) \tag{2}$$

Resistivity

$$\rho = (R_s xt) = 4.53\left(\frac{V}{I}\right)t \tag{3}$$

and conductivity

$$\sigma = \frac{1}{\rho} \tag{4}$$

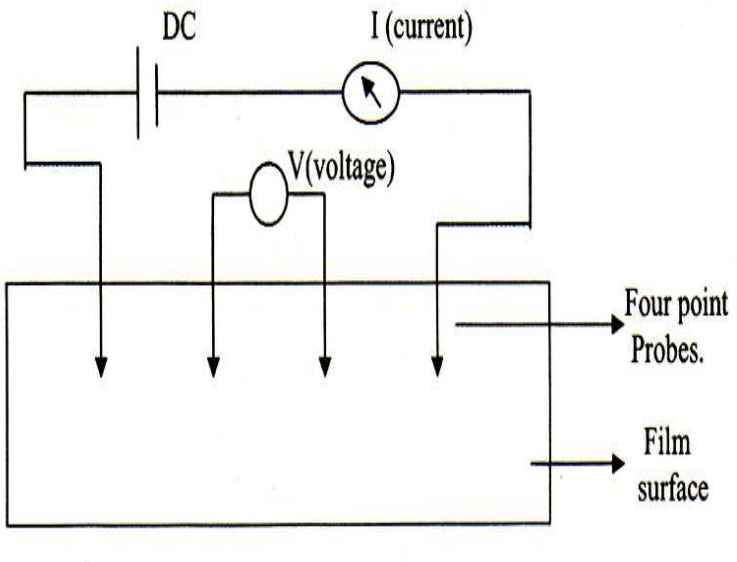

Figure 1. Four-Probe Technique

The probe can be made from thin tungsten wires (approximately 0.05cm diameter), which are sharpened electrolytically and fixed in a refractable plexi glass header by suitable cement. Commonly used spacing between the probes is s (0.159 cm). Thus, 4-point probe methods measure the average resistivity of the film on a substrate; provided film is either isolated from substrate or its resistivity is much lower than that of the substrate.

3. EXPERIMENTAL

Three source modified activated reactive evaporation unit shown in Fig.2 was used to deposit Al films on glass substrates. Aluminum thin films with thickness 0.0165 μm, 0.0620 μm, 0.1068 μm and 0.1564 μm were deposited in chamber with pressure approximately $210 - 6\bar{m}$. Tungsten coil was used to evaporate the high purity Al metal. Glass substrates were cleaned using distilled water, then by ethanol in ultrasonic bath and finally with the low pressure glow discharge. The thicknesses of the films were controlled during deposition by a quartz crystal and thickness measured by DTM thickness monitor model 101. The deposition LT (Low-Tension) current for all thickness of thin films was taken about 40-50A. The deposition rate in all thickness of the films was about 10 A^0/sec. The rotary pump reduced pressure from atmospheric to 0.001 mbar then the diffusion pump was started for the further reduction in pressure. The diffusion pump decreased the pressure from $0.001barm$ to $2x10^{-6}\bar{m}$. The desired thickness of the films were obtained on glass substrates and they were taken for resistance measurement.

Figure 2. Resistive thermal evaporation unit for deposition of Al thin films

The prepared Al thin film is placed inside the four probe set up. The outer pins are connected to the current source and the inner pins are connected to the voltage source.

Initial adjustments and observations:

1. Switch on DMV-001 and adjust zero on the panel at $10mV$ range, with the zero adjustment knob

2. Switch on $CCS - 01$ and set the current at zero and then again check the reading of $DMV -$

001 and adjust zero if required

3. Now increase the current gradually in $CCS01$ from 10 to $200mA$ in steps of $10mA$ and note down the corresponding voltage from $DMV001$. From the current and voltage values, the sheet resistance can be calculated using equation (2) and electrical conductivity can be obtained by equation (4).

4. RESULTS AND DISCUSSION

The variation of electrical resistivity with films thickness is shown in Fig.3. It shows that with increase in thickness of Al thin films, the resistivity decreases. Figure 4 shows the plot of conductivity as a function of film thickness. Similarly, sheet resistance decreases when films thickness increases as shown in Fig. 5. The resistivity of pure aluminum is $2.65x10^{-8}\Omega\dot{m}$ and the resistivity of thin films is more than that of bulk which is evident from Table I. High resistivity values in thin films can be attributed to fabrication process in which lattice defects, grain boundaries, impurities and uneven surfaces occur. These characteristics become predominant when the films are very thin and result in increase in the resistivity.

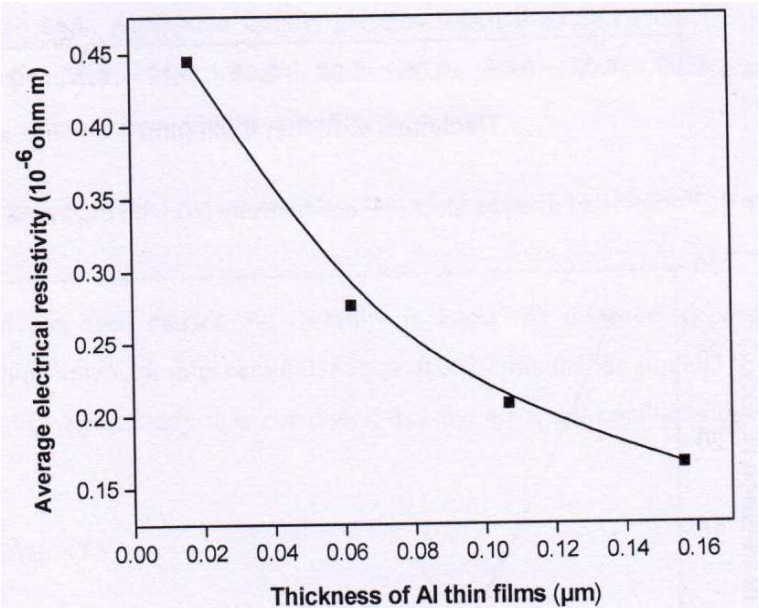

Figure 3. Variation of average electrical resistivity (ρ) with thickness of Al thin films

Unlike the properties of bulk materials, the resistivity, conductivity and sheet resistance in the thin film depends on several factors such as rate of deposition, thickness, temperature and grain boundaries [12].

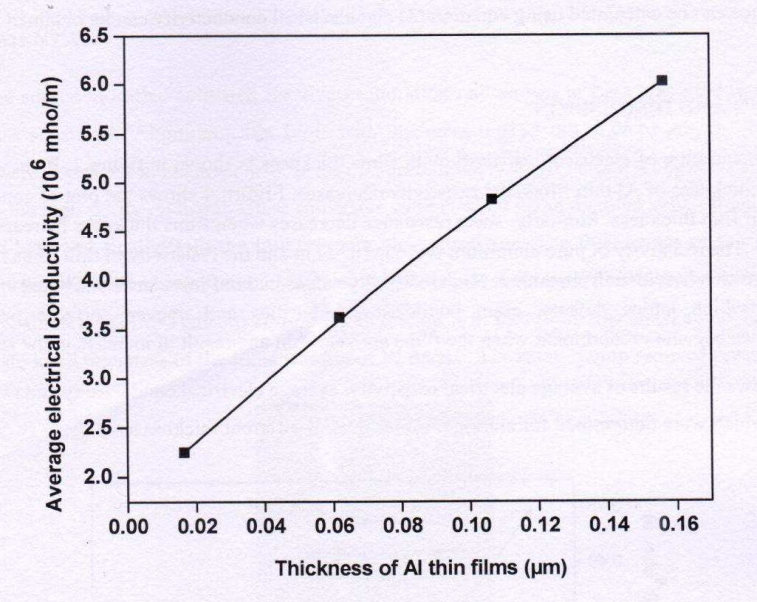

Figure 4. Variation of average electrical conductivity (ρ) with thickness of Al thin films

Table 1 shows the results of average electrical resistivity, average electrical conductivity and average sheet resistance which were determined for aluminum thin films of different thicknesses.

As the thickness of the film decreases, the electron collisions with surfaces become important. Such confinement effect due to film thickness is clearly observed on Al thin films whose electrical resistivity values are higher than bulk. Aluminum usually presents a native oxide film (Al2O3) when exposed to atmospheric pressure, which changes substantially its surface properties. As can be seen in figures 3 - 5, measured , and Rs values show variation with film thickness.

Table 1. Average electrical resistivity, average electrical conductivity, sheet resistance and thickness of Al thin films

Sl. No.	Al thin films samples	Thickness of Al thin films $t(\mu m)$	Average electrical resistivity $\rho(10^{-6}\Omega m)$	Average electrical conductivity σ $(10^{-6}mho/m)$	Average sheet resistance $R_s(\Omega)$
1	Sample 1	0.0165	0.4448	2.2475	26.9603
2	Sample 2	0.0620	0.2761	3.6212	3.6467
3	Sample 3	0.1068	0.2073	7.8229	1.9414
4	Sample 4	0.1564	0.1661	6.018	1.062

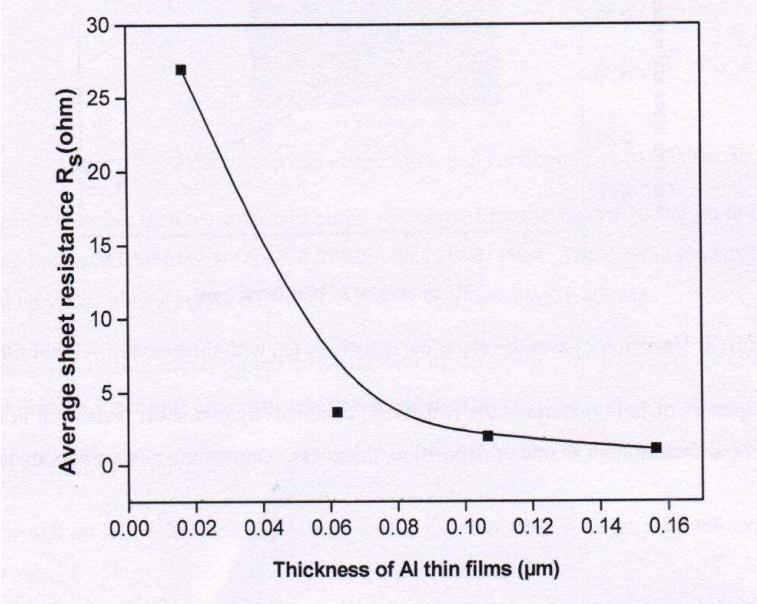

Figure 5. Variation of average sheet resistance (R_s) with thickness of Al thin films

5. CONCLUSION

Investigation has been carried out carefully to know the thickness dependence of electrical conductivity of Al thin films with thickness 0.0165 μm, 0.0620 μm, 0.1068 μm and 0.1564 μm deposited on glass substrates. From this study it is concluded that the electrical conductivity increases with film thickness.

Acknowledgements

The authors are thankful to Prof. Habibuddin Shaik, HOD and Mr. Satish, research scholor, Department of physics NMIT, Bangalore for providing us thin film coating facility and their timely suggestion and encouragement.

References

[1] CC. Cheng and CC. Lee, J Opt. Quant. Electron 28, 1583 (1996).

[2] G .Civrac, S. Msolli , J. Alexis, O. Dalverny, and H.Schneider, Electronics Letters 46, 791 (2010).

[3] S. Ishihara and T. Hirao, Thin Solid Films 155, 325 (1987).

[4] M.A. Green, Solar Cells: Operating Principles, Technology, and System Applications: Prentice-Hall (1982).

[5] J. Muller, B. Rech, J. Springer and M. Vanecek, Solar Energy 77, 917 (2004).

[6] J. Nelson, The Physics of Solar Cells, Imperial College Press (2003).

[7] M.L. Green, R.A. Levy, R.G. Nuzzo, and E.Coleman,Thin Solid Films 114, 367 (1984).

[8] K. Wijekoon, H. Mungekar, M. Stewart, P. Kumar, J. Franklin, M. Agrawal, K. Rapolu, Y. Fei, Z. Yi, A. Chan, M. Vellaikal, L. Xuesong, D. Kochhar, Z. Lin, D. Tanner, and V.DabeerH. Ponnekanti, IEEE 38th Photovoltaic Specialists Conference (PVSC), June 3-8-th 2012, Texas.USA.

[9] P.K. Shetty, N.D.Theodore, J. Ren, J. Menendez, H.C. Kim, E. Misra, J.W. Mayer, and T.L. Alford, Materials letters, 59,872(2005).

[10] W.E. Beadle, J.C.C. Tsai, and R.D. Plummer, Integrated R.D. Plummer quick Reference manual for Silicon. Integrated circuit Technology, Wiley, NewYork, 1985.

[11] Charles A. Bishop, Process Diagnostics and Coating Characteristics in Vacuum Deposition onto Webs, Films and Foils (Second Edition), 2011.

[12] A.I. Oliva, F. Aviles, and O. Ceh, Physical properties of AU and AL thin films measured by resistive heating, Surface Review and Letters, Vol.12, No.1(2005),101- 106, World Scientific Publishing Company.

STUDENT JOURNAL OF PHYSICS

Volume 9 **Number 1** **2022**

CONTENTS

ARTICLES